The Journal of Chemical Physics

AIP Publishing

An experimental and computational view of the photoionization of diol water clusters

Anna Wannenmacher[1,2], Wenchao Lu[1b], Chandika Amarasinghe[1c], Frank Cerasoli[2], Davide Donadio[2*], Musahid Ahmed[1*].

[1] Chemical Sciences Division, Lawrence Berkeley National Laboratory, Berkeley, California 94720, USA

[2] Department of Chemistry, University of California, Davis, California 95616, USA

mahmed@lbl.gov, ddonadio@ucdavis.edu

Present affiliation:

[b] CSIRO Environment, Urrbrae, South Australia 5064, Australia

[c] Thermo-Fisher, San Jose, CA, USA

The Journal of Chemical Physics

ABSTRACT

In the interstellar medium, diols and other prebiotic molecules embed onto icy mantles surrounding dust grains. Water in the ice may affect the reactivity and photoionization of these diols. Ethylene glycol (EG), 1,2-propylene glycol, and 1,3-propylene glycol clusters with water clusters were used as a proxy to study these interactions. The diol water clusters were generated in a continuous supersonic molecular beam, photoionized by synchrotron-based vacuum ultraviolet light from the Advanced Light Source, and subsequently detected by reflectron time-of-flight mass spectrometry. The appearance energies for the detected clusters were determined from the mass spectra, collected at increasing photon energy. Clusters of both diol fragments and unfragmented diols with water were detected. The lowest energy geometry optimized conformers for the observed EG water clusters and EG fragment water clusters have been visualized using density functional theory (DFT), providing insight into hydrogen bonding networks and how these affect fragmentation and appearance energy. As the number of water molecules clustered around EG fragments (m/z 31 and 32) increased, the appearance energy for the cluster decreased, indicating a stabilization by water. This trend was supported by DFT calculations. Fragment clusters from 1,2-propylene glycol exhibited a similar trend, but with a smaller energy decrease, and no trend was observed from 1,3-propylene glycol. We discuss and suggest that the reactivity and photoionization of diols in the presence of water depend on the size of the diol, the location of the hydroxyl group, and the number of waters clustered around the diol.

INTRODUCTION

Diols, alcohols with 2 hydroxyl groups, in the interstellar medium, may have acted as prebiotic molecules, participating in reactions forming basic building blocks of life, such as amino acids. The diol ethylene glycol (EG) has been detected in space, both in the interstellar medium (ISM) as well as in cometary ices, specifically in the hot core-like region Orion-KL[1] and in the star-forming region G31.41+0.31.[2] EG may also have played a role in the formation of comets[1] and is thought to adsorb onto interstellar ice, which forms on the surface of dust grains and other solar system objects.[3] Vacuum ultraviolet (VUV) light in the ISM can photoionize embedded molecules, forming cations as well as fragments, which may react forming larger prebiotic molecules. To better understand and predict these reactions, it is necessary to learn how water surrounding EG and other diol molecules affects the reactivity and ionization of the diol and to understand the role of hydrogen bonds between the hydroxyl groups and water. Unraveling hydrogen bonding between water and diols also has a technological relevance. EG water solutions have anti-icing properties and play important roles as cryoprotectants in biological systems, such as for proteins[4], as well as in superconductors, sensors, and batteries. When EG was added to the aqueous electrolyte $ZnSO_4$ a conductivity of 6.9 mS/cm was obtained at -40 ^oC[5] and when it was added to $Mg(ClO_4)_2$, the reduction in freezing point resulted in a device with advanced long-term cycling stability.[6] With the addition of EG water solutions to agar, aluminum-air batteries, and zinc-ion batteries have been shown to function at low temperatures.[7, 8]

Here we study the photoionization of clusters with water molecules and three diol molecules, EG, $(CH_2OH)_2$, 1,2-propylene glycol (12PG, $CH_3CH(OH)CH_2OH$), and 1,3-propylene glycol (13PG, $CH_2OHCH_2CH_2OH$, with synchrotron-based VUV photoionization mass spectrometry. 1,2 and 1,3-propylene glycols will at times be referred to jointly as propylene glycol (PG).

The dielectric behavior[9] and thermodynamic properties[10] of propylene glycol water mixtures have been analyzed, as has a comparison of the dielectric properties of EG and propylene glycol.[11] Using theoretical calculations, the thermodynamic properties of EG water mixtures were determined[12] and used to model the microsolvation effect on ethylene glycol[13] as well as determine the structure of the ethylene glycol water mixture[14] along with that of the pure liquid.[15] The hydrogen bond networks of pure liquid EG as well as EG and water have been examined using near-infrared spectroscopy[16,17] and Raman spectroscopy[16]. Both the IR and Raman spectroscopy experiments found that the structure is determined by the hydrogen bonds formed between the hydroxyl groups and water and the nature of the bonding depends on concentration.[16-18] While there has been extensive work, both experimentally and theoretically, on liquid-phase EG water mixtures, little is known about the photoionization of gas-phase EG and propylene glycol water clusters, leaving a gap in understanding how water surrounding a diol affects the diol's ionization and fragmentation when exposed to VUV light.

Single photoionization is the least complicated photoionization method and is most commonly accomplished using VUV light,[19] which provides an efficient and soft method for ionizing molecules.[20] Using this method, the ionization energy (IE), appearance energy (AE), photoioinization intensity curves, and energetics of molecules can be determined.[20] The tunable nature of the VUV radiation results in precise threshold ionization, with little excess internal energy

imparted to the ion.[20] The thermodynamics and bonding properties of water clusters have been analyzed using tunable VUV radiation (10 – 14 eV) with detection by a reflectron time-of-flight mass spectrometer. The neutral clusters were photoionized forming an unstable cation cluster, $[(H_2O)_n^+]$, which underwent a redistribution, forming protonated clusters containing up to 79 molecules. Photoionization intensity curves were obtained, and from these, AEs were determined. A decrease in AE was observed as the cluster size increased. The most substantial drop was observed when the cluster size increased to 4 water molecules' causing AE to converge to an asymptote around 10.6 eV.[21]

The effects of hydrogen bonding networks on fragmentation dynamics have been observed through the photoionization of alcohols and sugars. VUV photoionization of the simplest alcohol, methanol, in the presence of water, has been studied. Below the ionization energy of methanol, the mass spectrum was dominated by protonated methanol clusters, $(CH_3OH)_nH^+$ (n = 1 – 12). When the concentration of water was increased, methanol-water clusters, $(CH_3OH)_n(H_2O)H^+$ (n = 2 – 11) formed.[22] Photoionization mass spectrometry of the larger alcohol glycerol has been performed, and fragmentation of the glycerol radical cation was found to occur via two channels. One channel proceeds through a six-membered hydrogen transfer transition state, forming a ternary intermediate, and the other channel proceeds via the cleavage of the C-C bond. The intermediate is composed of neutral water, neutral formaldehyde, and a vinyl alcohol radical cation, explaining why the first observed products result from water or formaldehyde loss.[23] Similar to glycerol, water elimination and fragmentation through a cyclic intermediate were observed with photoionization mass spectrometry of the sugar deoxyribose. In this case, most of the fragmentation occurred when the cyclic molecule was unfurled by breaking a C-C bond. This caused two hydroxyl groups to come close together, resulting in water elimination.[24] Hydrogen bonding in glycerol was further investigated by performing photoionization mass spectrometry of glycerol water clusters. The AEs of certain fragments were found to be like those seen with pure glycerol, while for other fragments the AE was found to depend upon both cluster composition and water concentration in the beam. Theory calculations predicted certain barrierless chemical processes when glycerol water clusters were photoionized, which were not observed to occur with pure glycerol.[25]

There are some reports on the thermal decomposition and dissociative ionization of pure EG performed via VUV photoionization mass spectrometry. From this, the appearance energies of the observed fragments were determined, and possible formation channels for the fragments were proposed via theory calculations.[26] Complementing this work, Kumar et al. performed DFT theory calculations to determine the structure, stability, and spectral properties of pure EG as well as EG-water clusters, which up until this writing had not been studied experimentally in the gas phase. These calculations found that, due to electrostatics and polarization, interactions between water and EG are preferred over those between pure EG.[27] To further our understanding of the photoionization of alcohol-water clusters, we performed photoionization mass spectrometry experiments of ethylene glycol water clusters, 1,2-propylene glycol water clusters, and 1,3-propylene glycol water clusters in a molecular beam paired with theoretical calculations on both neutral and ionized EG water clusters. Via this work, the effect of the hydrogen-bond network formed when water clusters around diols is understood through the changes in ionization energy, appearance energy, and fragmentation of the diols in the clusters.

METHODS

Experimental Details

The experiment was performed with a reflectron time-of-flight mass spectrometer containing a continuous supersonic expansion molecular beam source connected to a 3-meter vacuum monochromator and attached to the Chemical Dynamics Beamline (9.0.2) located at the Advanced Light Source. For a detailed description of the instruments, refer to previous studies.[21, 28-29] The diol of interest, either EG or PG, is placed in a stainless-steel nozzle, vaporized by a cartridge heater, and entrained in an argon carrier gas seeded with water vapor. The gas mixture passes through a 50 μm nozzle source and supersonically expands into a vacuum chamber, yielding the desired diol water molecular beam. This beam is extracted through a skimmer into a differentially pumped interaction region where the clusters are exposed to and ionized by VUV synchrotron radiation. The ionized fragments are then detected using a reflectron time-of-flight mass spectrometer. Mass spectra are recorded at photon energies between 9.0 and 12.5 eV every 50 meV. Photoionization intensity curves, which show ion count versus photon energy (in eV), of the diol water clusters are obtained by integrating over the peaks in the mass spectrum at each photon energy after being normalized by the photon flux.

Computational Details

Theoretical calculations were performed on the EG water cluster system. The optimized geometries of the observed clusters were determined through a conformation search using the semi-empirical quantum chemistry package Crest.[30] The lowest energy conformer from this search was further optimized as both neutral and cation, with the cation geometry determined by setting the total charge to +1, using Q-Chem[31] at the ωB97X-D/6-311+G-(2d,p) level of theory. For geometry optimization, the hybrid functional ωB97X-D reproduces the intermolecular interactions well given its range-separated exact exchange and dispersion corrections.[32] Single-point calculations were carried out with the ωB97X-V functional and the def2-TZVPPD basis set to determine vertical and adiabatic ionization energies. This computational framework was chosen due to its enhanced atomic orbital basis set. Appearance energies were calculated using the calculated energies (E) for neutral EG (m/z 62), neutral m/z 31, and cation m/z 31, as shown in equation 1 below, where *m*, *n*, and *k* represent the number of water molecules in the cluster. Starting from a cluster consisting of one EG and *m* water molecules, the AEs of fragment m/z31$(H_2O)_n^+$ ionized clusters were calculated at the ωB97X-V/def2-TZVPPD level of theory.

$$AE(m/z31(H_2O)_n^+) = E(m/z31(H_2O)_{m-n}) + E(m/z31(H_2O)_n^+) - E(m/z62(H_2O)_m) \quad (1)$$

More details on this calculation are given in the results and discussion section.

RESULTS AND DISCUSSION

Mass Spectra of EG

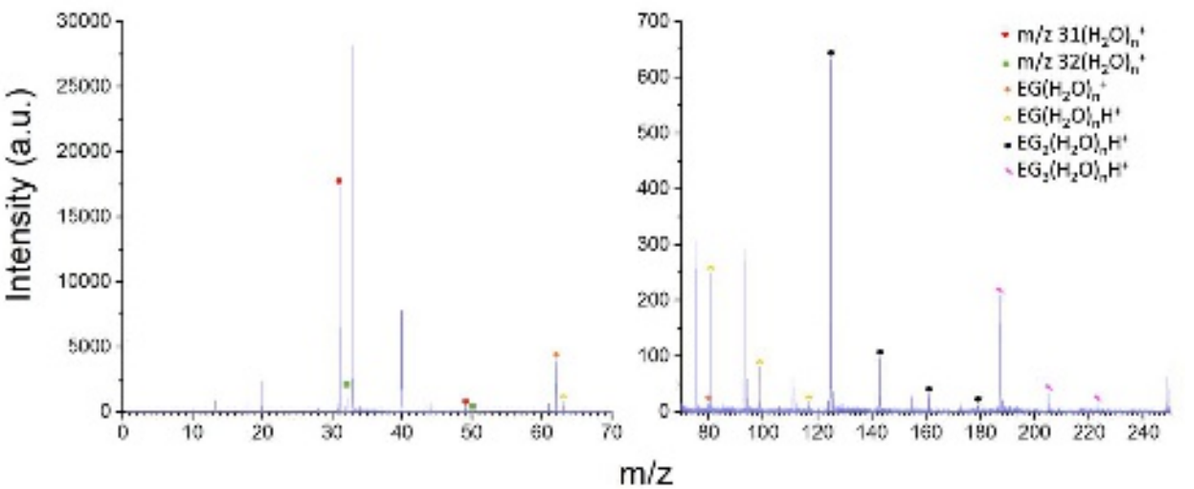

Figure 1 40% EG mass spectrum recorded at 12.0 eV. The cluster series for m/z 31$(H_2O)_n^+$, m/z 32$(H_2O)_n^+$, m/z 62$(H_2O)_n^+$, m/z 63$(H_2O)_n^+$, m/z 125$(H_2O)_n^+$, and m/z 187$(H_2O)_n^+$ are indicated with colored dots. Ethylene glycol has a mass of 62 amu.

The concentration of EG to water in the molecular beam was adjusted by changing the temperature of the nozzle as well as the pressure of the backing Ar (resulting in the peaks at m/z 40, Ar^+, and m/z 20, Ar^{2+}) gas. The mass spectrum taken with 40% EG at 12 eV is shown in Figure 1, where the x-axis has been split over 2 plots to better show the intensity of the peaks. The mass spectra are dominated by EG water clusters, both protonated and unprotonated, as well as EG fragments and fragment water clusters. The cluster series m/z 31$(H_2O)_n^+$, m/z 32$(H_2O)_n^+$, m/z 62$(H_2O)_n^+$, m/z 63$(H_2O)_n^+$, m/z 75$(H_2O)_n^+$, m/z 125$(H_2O)_n^+$, and m/z 187$(H_2O)_n^+$ are indicated with colored dots. Pure water clusters (such as the prominent peak m/z 36, which is from water dimer) as well as other peaks (such as m/z 18) are observed in the mass spectra but are not the focus of this paper and so are not discussed further.

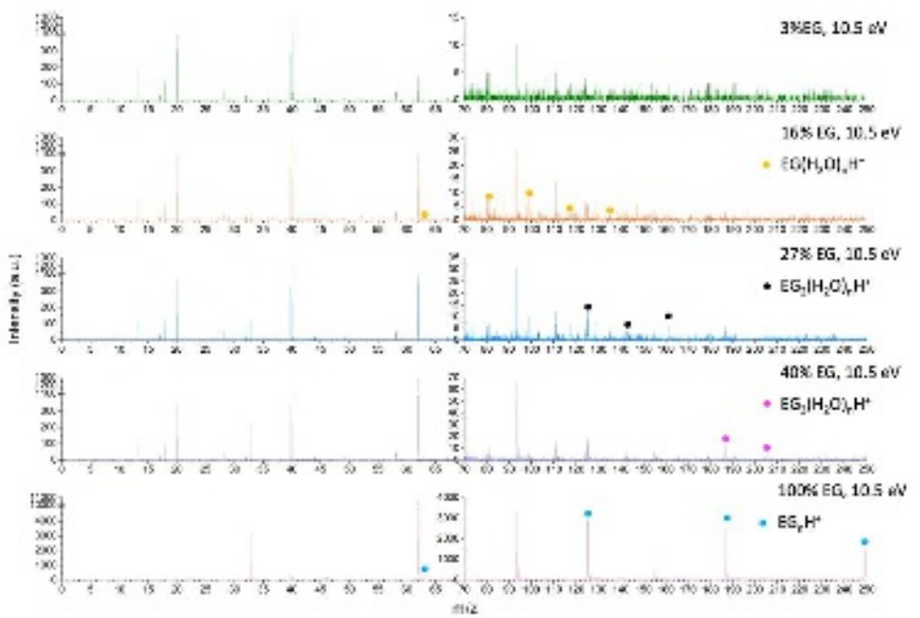

Figure 2 Mass spectra of EG water clusters recorded at 10.5 eV at EG mole fractions of 3%, 16%, 27%, and 40%. Monomer, dimer, and trimer protonated EG water clusters are indicated with colored dots.

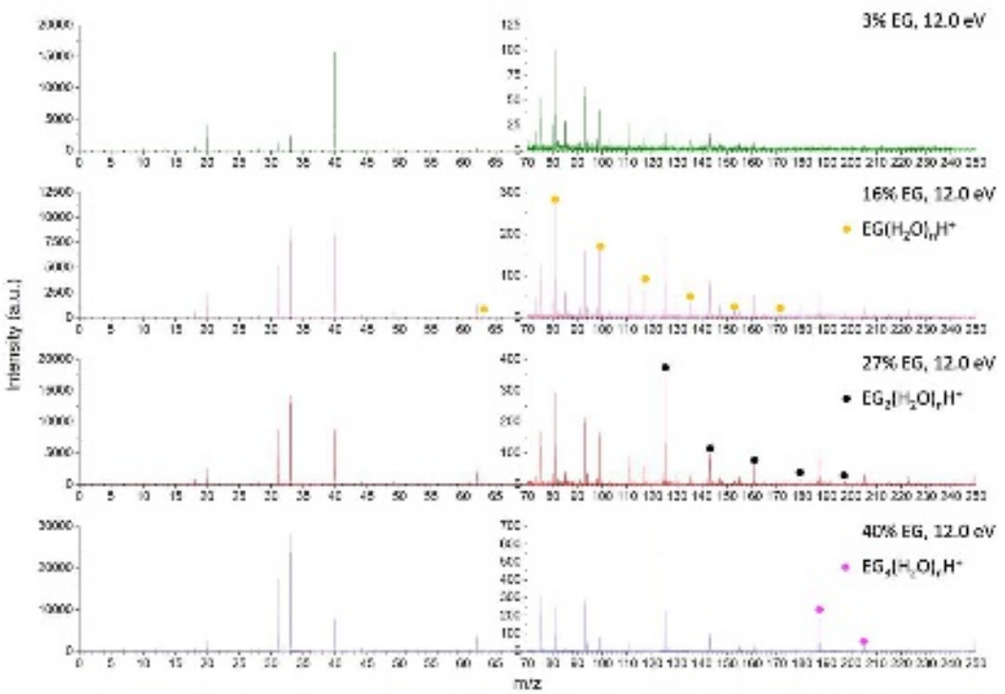

Figure 3 Mass spectra of EG water clusters recorded at 12.0 eV at EG mole fractions of 3%, 16%, 27%, and 40%. Monomer, dimer, and trimer protonated EG water clusters are indicated with colored dots.

The concentration of EG in the molecular beam as well as the photon energy affect the intensity of clusters. This can be observed in figures 2 and 3 which show mass spectra obtained at different mole fractions of EG, specifically 3%, 16%, 27%, and 40%. All mass spectra in Figure 2 were taken with a photon energy of 10.5 eV and in Figure 3 with a photon energy of 12.0 eV. Monomer, dimer, and trimer protonated EG water clusters are indicated in these figures.

Along with fragments m/z 31 and m/z 32 (indicated in Figure 1), other EG fragments were observed with masses m/z 43, 44, 45, and 61. A previous VUV photoionization study of pure EG determined the formation channels and chemical identities of these fragments.[26] Based upon this, the fragments are attributed as follows: m/z 31 is CH_2OH^+, m/z 32 is CH_3OH^+, m/z 43 is CH_3CO^+, m/z 44 is CH_2CHOH^+, m/z 45 is CH_3CHOH^+, and m/z 61 is $C_2H_5O_2^+$.

In the mass spectrum shown in Figure 1, the peak to the left of m/z $125(H_2O)_n^+$ (which corresponds to m/z $EG_2(H_2O)_nH^+$) is from unprotonated EG dimer water clusters. Larger clusters with up to 5 waters around EG, $EG(H_2O)_5H^+$, and $EG_2(H_2O)_5H^+$, were observed, but are not highlighted in Figure 1 due to the low intensity of their corresponding peaks. The signal from these largest clusters is found to be too noisy to give useful information, so these clusters are omitted from subsequent tables.

Figure 4 shows the sum of the cluster series as a function of the EG mole fraction taken at 12.0 eV. EG fragments represent the sum of masses m/z 31, 32, 33, 43, 44, 45, 61. All clusters are observed to increase with the concentration of EG. With increasing EG concentration, the intensity of fragment cluster m/z 31$(H_2O)^+$ increases more rapidly than the intensity of EG water clusters.

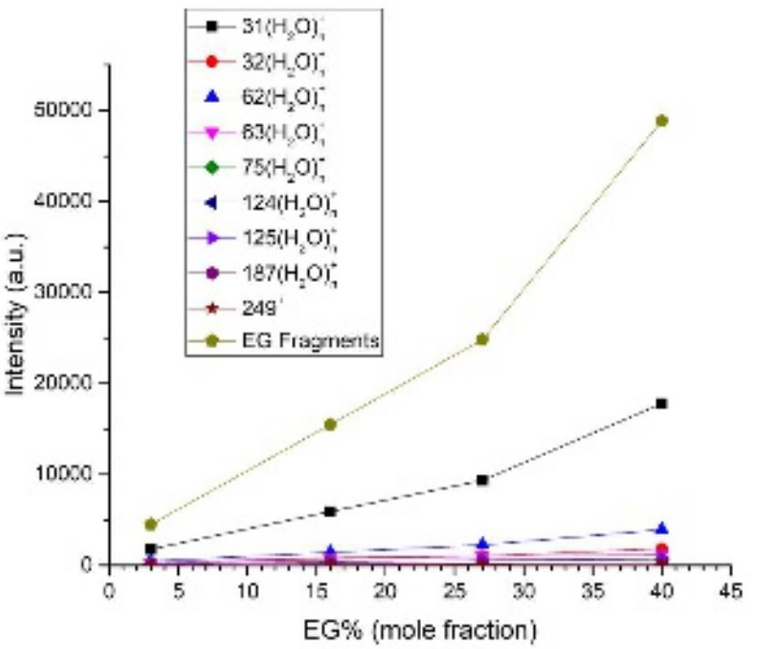

Figure 4 Sum of intensities of each cluster series as a function of EG mole fraction, recorded at 12.0 eV. The EG fragments summed are m/z 31, 32, 33, 43, 44, 45, 61.

Lowest Energy Geometries of EG Water Clusters

The lowest energy conformers of the clusters in the molecular beam were determined and optimized as outlined in the methods section and are shown in Figures 5, 6, and 7.

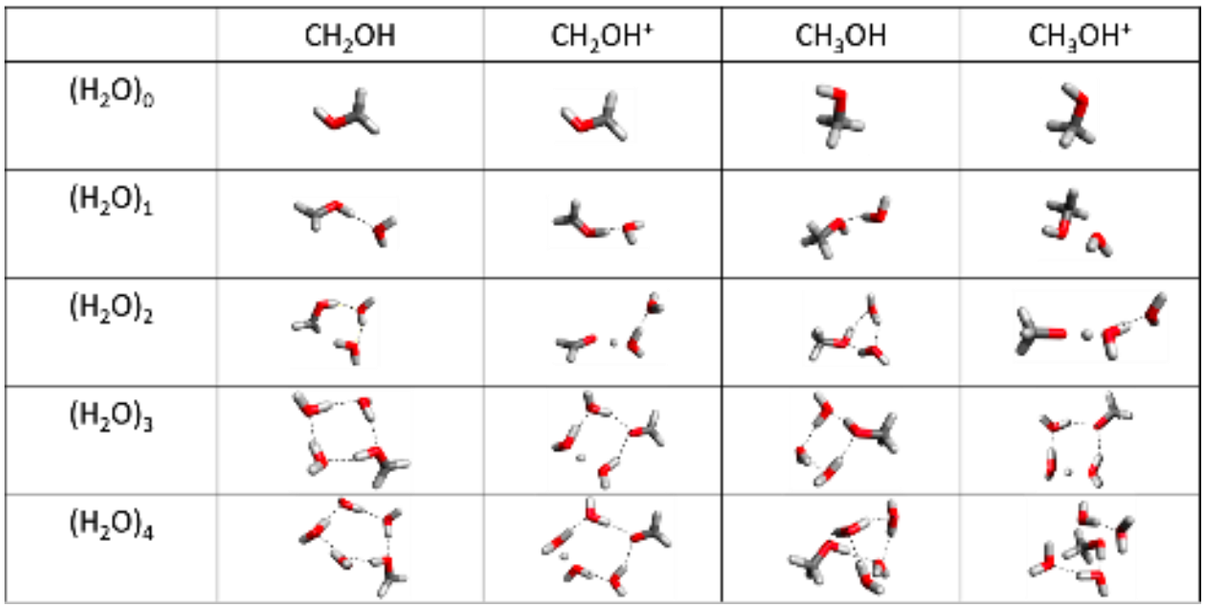

Figure 5 Geometry optimized lowest energy conformers for fragments with mass 31, both neutral (CH_2OH) and cation (CH_2OH^+), and mass 32, neutral (CH_3OH) and cation (CH_3OH^+). These conformers were identified using the semi-empirical quantum chemistry package Crest and then further optimized using Q-Chem (ωB97X-D/6-311+G-(2d,p)).

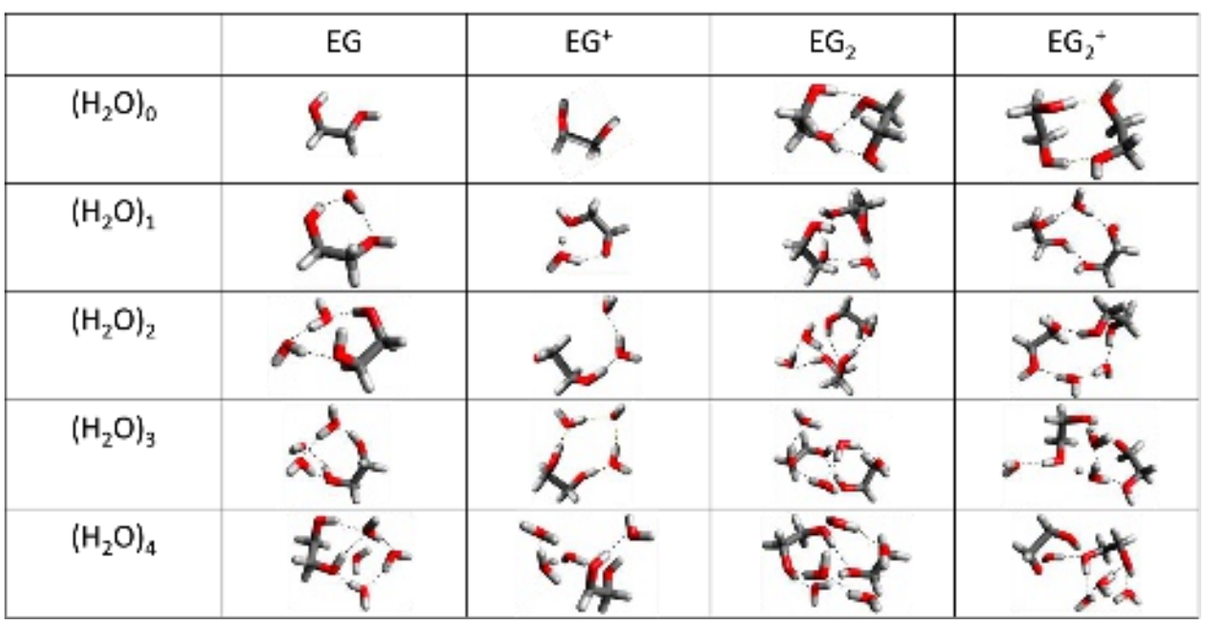

Figure 6 Geometry optimized lowest energy conformers for both neutral and cationic EG (mass 62) and dimer EG (mass 124). These conformers were identified using the semi-empirical quantum chemistry package Crest and then further optimized using Q-Chem (ωB97X-D/6-311+G-(2d,p)).

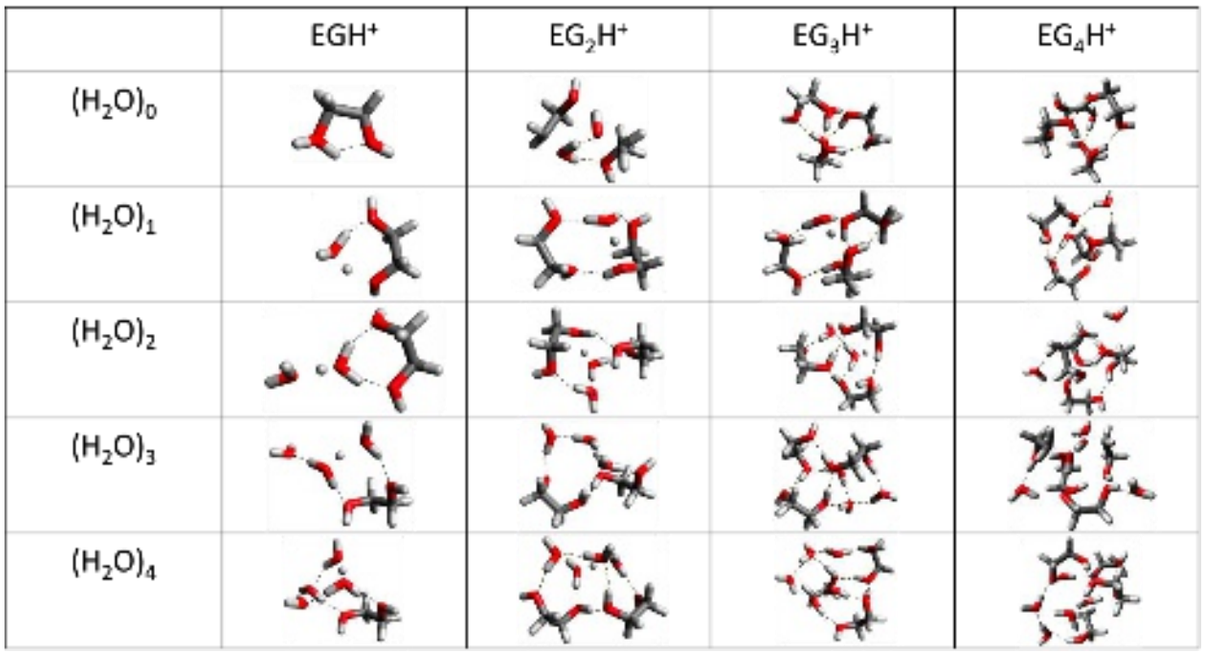

Figure 7 Geometry optimized lowest energy conformers of cationic protonated EG monomer (mass 63), dimer (mass 125), trimer (mass 187), and tetramer (mass 249). These conformers were identified using the semi-empirical quantum chemistry package Crest and then further optimized using Q-Chem ωB97X-D/6-311+G-(2d,p).

Using the calculated energies of the optimized geometries of the clusters, the appearance energies of the ionized clusters were calculated and will be discussed in detail later. The structural models reveal the most energetically favorable hydrogen bonding patterns between EG and the water network. When EG is neutral, water molecules are observed to connect the two OH groups forming a pathway or water wire which makes for easy proton hopping between the two OH groups. When the fragments CH_2OH^+ and $CH_3OH^+$are surrounded by three water molecules, the proton from the OH group of EG detaches and is shared between two water molecules forming a Zundel ion, which is the ion formed when 2 water molecules share a proton between them. This Zundel ion is also observed to form in protonated clusters with up to four EG molecules.

Photoionization Intensity Curves and Appearance Energies (AE)

From the mass spectra, recorded every 50 meV, photoionization intensity curves were obtained for all clusters at each concentration of EG (3%, 16%, 27%, and 40%) and are given in the SI, figures S1 through S6. As an example, one photoionization intensity curve for fragment m/z 31 water clusters, taken with 27% EG in the molecular beam, is shown in Figure 8. The arrows indicate the location of the appearance energy, which for this cluster varies substantially with cluster size. This will be discussed in detail later.

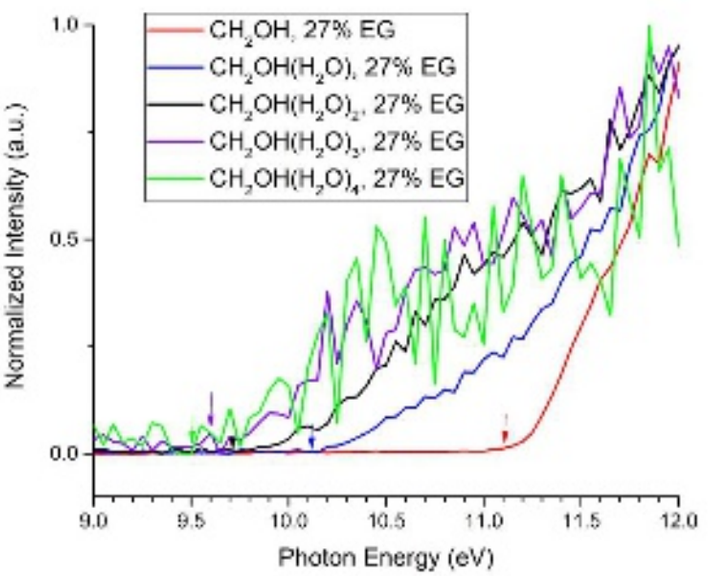

Figure 8 Photoionization intensity curve for fragment m/z 31 water clusters with 27% EG in the molecular beam. Each curve is normalized to the largest y value to make comparisons between the curves easier. The arrows indicate the location of the appearance energy.

From the photoionization intensity curves, the appearance energies for the clusters, as a function of mole fraction, were determined and are given in Table 1, along with experimental and calculated AE values from reference 24. We define appearance energy as the energy needed to ionize and potentially fragment the gas phase molecule or cluster. AE is determined by visually identifying the first major rise above the baseline as has been done in previous work.[33] Based upon the determination method, an uncertainty of ±0.1 in the reported appearance energy is assumed. This error value varies slightly depending upon the noise in the photoionization intensity curve with the size in error increasing as the noise in the spectrum increases. The values determined from the curves with the lowest signal-to-noise are identified in Table 1 by an *. The variation in error overall is small so a general error of ±0.1 is justified. This paper focuses on large changes in AE (on the order of 1 eV), which are much larger than the error.

The concentration of EG in the molecular beam showed no effect on appearance energy indicating that the concentration of water does not affect fragmentation. By contrast, the appearance energy is dependent upon the size of the cluster. The intensity of the clusters is directly related to the photon energy, as can be observed in Figures S7 through S10 in the SI. The plots are shown for clusters with up to 4 waters, though not all clusters were observed to be this large.

Table 1 Appearance energies (AE) in eV of EG clusters as well as fragment clusters observed at different mole fractions of EG with an error of ±0.1 eV. The error in the appearance energies from reference 20 is ±0.05 eV. A - indicates that the signal-to-noise ratio was not good enough to obtain a conclusive AE value. * indicates that the photoionization intensity curve has a low signal to noise resulting in high uncertainty in the AE value. The identity of the m/z # is indicated by square brackets.

	AE (eV) as a function of EG%					
	3%	6%	27%	40%	Experimental[26]	Calculated[24]
m/z 31^+	11.1	11.1	11.1	11.1	11.12	11.18
m/z $31(H_2O)^+$	10.2	10.2	10.1	10.1		
m/z $31(H_2O)_2^+$	9.8	9.8	9.7	9.8		
m/z $31(H_2O)_3^+$	9.7	9.7	9.6	9.6		
m/z $31(H_2O)_4^+$	9.6*	9.6	9.5	-		
m/z 32^+	10.8	11.1	11.2	11.2	11.42	11.47
m/z $32(H_2O)^+$	10.4	10.3	10.3	10.4		
m/z $32(H_2O)_2^+$	9.9*	9.9	9.9*	9.9*		
m/z 33^+	10.2	10.3	10.2	10.2	10.45	11.77
m/z 43^+	10.3	10.6	10.3	10.5	10.64	11.43
m/z 44^+	10.7	10.7	10.7	10.7	10.64	10.80
m/z 45^+	10.5	10.5	10.3	10.5	11.00	10.80
m/z 61^+	10.9	10.9	10.9	10.9	10.84	10.77
m/z 62^+, [EG]	9.9	9.9	9.9	9.9	9.85	9.77
m/z $62(H_2O)^+$	-	9.6*	9.6	-		
m/z $62(H_2O)_2^+$	9.7*	9.7*	9.7*	9.7*		
m/z 63^+, [EGH]	10.1	10.1	10.1	10.1*		
m/z $63(H_2O)^+$	10.4	10.2	10.2	10.2		
m/z $63(H_2O)_2^+$	10.0*	9.9	9.8	9.8		
m/z $63(H_2O)_3^+$	10.0*	9.5	9.8	9.6*		
m/z $63(H_2O)_4^+$	-	9.6	9.6	-		
m/z 124^+, [EG_2]	9.5	9.5	9.5	9.5		
m/z $124(H_2O)^+$	9.5*	9.5*	9.5*	9.5*		
m/z 125^+, [EG_2H]	-	9.9	10.0	9.9		
m/z $125(H_2O)^+$	-	10.1	9.6	9.6		
m/z $125(H_2O)_2^+$	-	9.8	9.7	9.7*		
m/z $125(H_2O)_3^+$	-	9.8	9.9	-		
m/z $125(H_2O)_4^+$	-	9.9*	-	-		
m/z 187^+, [EG_3H]	-	9.7	9.7	9.7		
m/z $187(H_2O)^+$	-	10.0	9.6	9.7		
m/z $187(H_2O)_2^+$	-	9.8*	9.7*	9.6*		
m/z 249^+, [EG_4H]	-	9.8	9.8	9.8		

Ionization Energy

Typically, the appearance energy obtained from a photoionization intensity curve for a cluster with hydrogen bonds would correspond to vertical ionization energy (VIE), which occurs when a neutral cluster absorbs a VUV photon causing a transition to a vibrationally excited ionic state with the same geometry as the neutral cluster. From there the cluster may relax, resulting in a geometry change, and the energy difference between this relaxed cation and the neutral molecule is the adiabatic ionization energy (AIE). Vertical and adiabatic ionization energies for the lowest energy geometry optimized conformers of EG water clusters and dimer EG water clusters were calculated and are shown in Table 2.

Table 2 Calculated adiabatic and vertical ionization energies for EG (m/z 62) clusters and EG dimer (m/z 124) clusters.

	EG (m/z 62)		EG Dimer (m/z 124)	
	Adiabatic IE (eV)	Vertical IE (eV)	Adiabatic IE (eV)	Vertical IE (eV)
$(H_2O)_0$	9.6	10.5	8.7	9.8
$(H_2O)_1$	9.3	11.4	8.5	10.1
$(H_2O)_2$	8.9	10.5	8.4	10.1
$(H_2O)_3$	8.3	9.7	8.3	10.4
$(H_2O)_4$	8.0	9.8	8.6	10.1

The larger the difference in energy between the adiabatic and vertical ionization energies, the worse the Frank-Condon Factor and therefore the greater the geometry change upon relaxation after ionization. In this case, the vertical and adiabatic ionization energies are not close indicating a change in geometry upon relaxation. This ionization process is outlined for EG water clusters in Figure 9 and for dimer EG (m/z 124) water clusters in Figure 10.

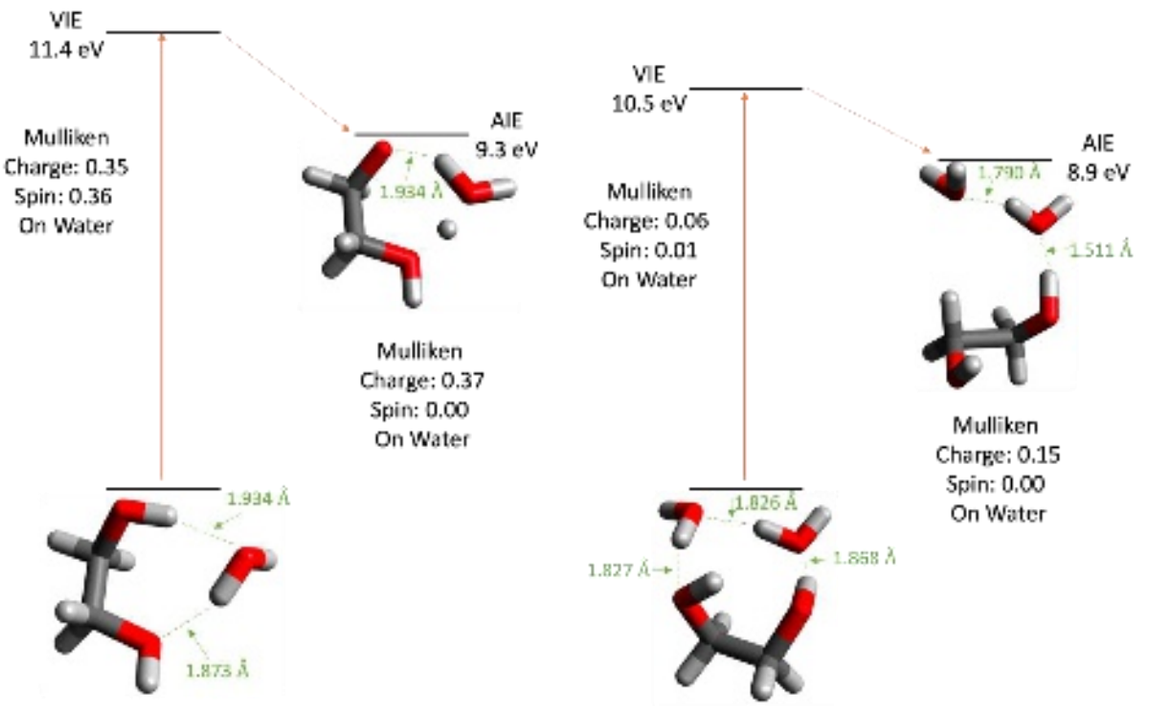

Figure 9 Vertical and adiabatic ionization of clusters $EG(H_2O)$ (left) and $EG(H_2O)_2$ (right)

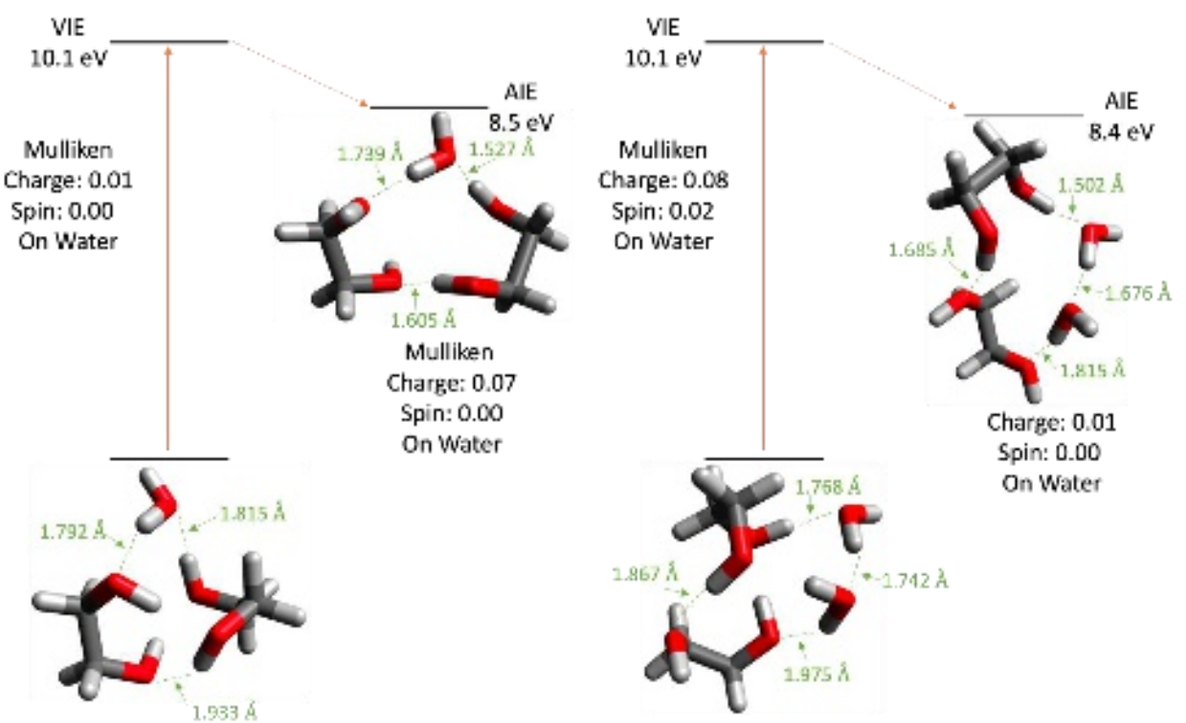

Figure 10 Vertical and adiabatic ionization of clusters $EG_2(H_2O)$ (left) and $EG_2(H_2O)_2$ (right)

In Figures 9 and 10 certain hydrogen bonds are labeled and the Mulliken charges and spins on water are given. The ionization process changes the hydrogen bonding networks and cluster geometries. The Mulliken charge and spin are obtained theoretically via a Mulliken population analysis and give an estimate of the partial atomic charges.[34] For the clusters shown at threshold, the majority of the charge and spin of the cluster is localized on EG indicating that when ionized, the charge prefers to stay on EG rather than moving towards water. Of the four clusters, water in cluster $EG(H_2O)^+$ has the highest charge and spin. Here, at 10.1 eV, no water ionization is observed, but at higher energies, water ionization would occur and this might result in a hole in the 3A" orbital as was seen in naphthalene water clusters and dimethyl uracil water clusters.[35-36]

Changes in AE with cluster size

As can be seen in Table 1, as cluster size around both protonated and unprotonated EG monomer, dimer, and trimer increases, the appearance energy decreases slightly and ultimately converges. This same trend was observed with glycerol water clusters,[25] PAH water clusters[35], and nucleobase water clusters.[37] A similar trend in decreasing AE was observed with increasing methanol molecules clustered around a single water molecule.[22] Pure EG (m/z 62) has an appearance energy of 9.9 eV, while an EG cluster with 2 waters has an appearance energy of 9.7 eV, a decrease of 0.2 eV, which is small given that the error in appearance energy is $\pm$ 0.1 eV. The appearance energies for fragments m/z 31 and 32 are over 1 eV higher than that of pure EG. The higher appearance energy is due to the additional energy needed to break the C-C bond of the unfragmented molecule or cluster after ionization. This process is outlined in Figure 11. In contrast to the unfragmented clusters, the appearance energy of the fragment water clusters is found to decrease substantially as cluster size increases, with a nearly 1 eV drop when 1 water is added to the fragment. Water surrounding the unfragmented molecule stabilizes the product so less energy is required to break the C-C bond and form the fragment.

Given the high energy of the VUV beam, it might be expected that water would evaporate during the fragmentation process. This is found not to be the case given the observed fragment clusters. To investigate this, the average excess energy (E_{excess}), which could cause water molecules to evaporate after ionization of the EG water clusters, was calculated as:

$$E_{excess} = AE - AIE$$

The average appearance energy (*AE*) for EG water clusters is 9.7 eV and the average AIE for these clusters is 9.3 eV giving an excess energy of 0.4 eV at the threshold. If this excess energy is higher than the binding energy of water in the cluster, then the water may evaporate. The binding energy of water in EG water clusters was determined following equation:

$$E_{bind} = E[EG(H_2O)_n]^+ - E[EG(H_2O)_{n-1}]^+ - E(H_2O)$$

where E is the electronic energy calculated as described in the methods section. The calculated binding energies are given in Table 3.

Table 3 Binding energies in eV, calculated at the ωB97X-V/def2-TZVPPD level of theory, of the *n*th water (*n* = 1 – 4) attached to EG$(H_2O)_n^+$ clusters.

	n = 1	*n* = 2	*n* = 3	*n* = 4
BE (eV) of EG$(H_2O)_n^+$	0.60	0.88	0.87	0.71

These binding energies are in the same ballpark as those found for methanol-water clusters and ethanol-water clusters.[38] The binding energy for EG$(H_2O)_n^+$ does not exhibit a clear trend, the value increases when the cluster increases from one water to two, stays about the same with three waters, and decreases with four waters. These binding energy values can be compared with a study that theoretically observed the trend in binding energy for neutral open-shell, neutral closed-shell, cationic, and anionic molecule water clusters with up to 4 water molecules. In general binding energy increased as the number of water molecules in the cluster increased. This was especially true for the cationic and anionic clusters, where cationic water clusters had the largest magnitude binding energies. This increasing trend did not always hold for neutral (both open and closed shell) molecule water clusters. When the water clusters were large, the most powerful interactive force was hydrogen bonding between the water molecules and little interaction occurred between water and the neural molecule.[39] The binding energies calculated for ethylene glycol water clusters are closest in absolute value to those for NH_4^+ water clusters (binding energy from DFT calculations are -0.82 eV, -1.43 eV, -0.62 eV, and -0.62 eV for clusters containing one to four water molecules, respectively). Neither of these clusters follows the trend of increasing binding energy as cluster size increases. The low binding energy of water to NH_4^+ is attributed to a lack of reaction when NH_4^+ is solvated. In these clusters, hydrogen bonding is maximized, but no proton from the NH_4^+ is lost to the water cluster resulting in no new chemical bonds.

The average binding energy is 0.76 eV, which is 0.36 eV higher than the excess energy and explains why at threshold energies, water did not evaporate during the fragmentation process, and therefore fragment water clusters were observed. At higher photon energies, above the threshold, fragment water clusters are still observed. The clusters in the molecular beam may have argon clusters around them, which may evaporate with the excess energy. Previous work looking at argon water clusters detected $(H_2O)_m^+$ and $(H_2O)_mH^+$, but did not detect $Ar_n(H_2O)_m^+$ nor $Ar_n(H_2O)_mH^+$.[40] At threshold, the excess energy was 0.2 eV and the binding energy converged to roughly 30 meV. This excess energy upon ionization is enough to evaporate 7 argon molecules, which explains the lack of detected argon water clusters. This argon water cluster finding lends support to the idea that the excess energy, when above the threshold of the EG water clusters, goes into evaporating argon clusters rather than evaporating the water cluster surrounding EG, as shown in Figure 6. The appearance of these EG water clusters indicates that, at least on the time scale of detection, the water clusters are not observing the ionization and fragmentation processes of EG.

The decrease in appearance energy as water clusters around fragments m/z 31 and m/z 32 indicates that the interaction between the water and EG is affecting both the ionization and fragmentation processes.

A suggested potential energy surface for the formation of this fragment is shown in Figure 11. This is based upon the appearance energy for fragment m/z 31 clusters being higher than the vertical ionization energy of EG. No transition state was observed when sampling the fragmentation process by stretching the C-C reaction coordinate and therefore no transition state is shown in Figure 11.

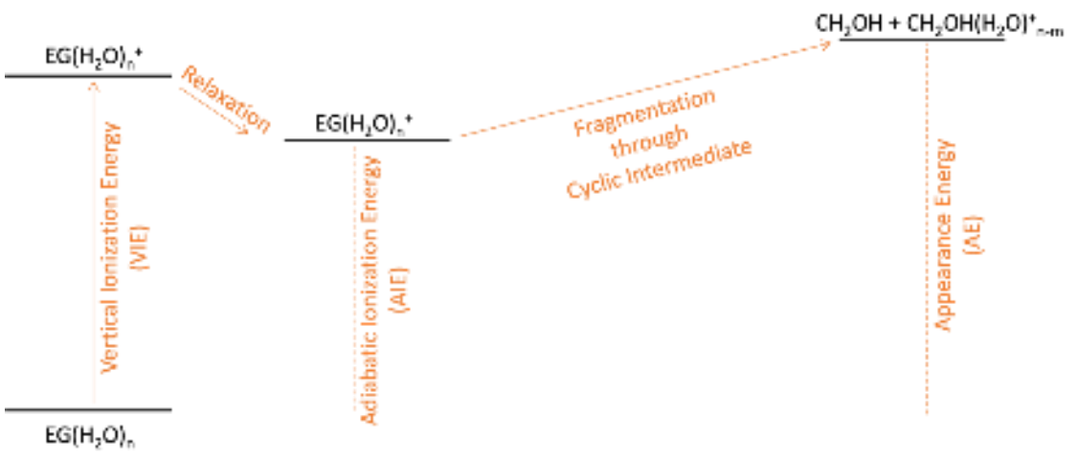

Figure 11 Potential energy surface for the fragmentation process of EG water clusters forming m/z 31 water clusters. This process is hypothesized to occur through a cyclic intermediate.

The appearance energy is calculated theoretically following equation 2 where *m*, *n*, and *k* represent the number of water molecules in the cluster and E is the electronic energy calculated as described in the methods section.

$$AE[\text{m/z } 31(H_2O)_n^+] = E[\text{m/z } 31(H_2O)_m] + E[\text{m/z } 31(H_2O)_n^+] - E(\text{m/z } 62(H_2O)_k) \quad (2)$$

The size of the EG water cluster producing the observed fragments is unknown, so the appearance energy for the clusters was determined using EG water clusters of different sizes. The determined values are shown in Table 4.

Table 4 Calculated appearance energy for m/z $31(H_2O)_n^+$. This table indicates that the final product is the determining factor in the energy, rather than the size of the reactant EG water cluster.

	m/z 31^+	m/z $31(H_2O)^+$	m/z $31(H_2O)_2^+$	m/z $31(H_2O)_3^+$	m/z $31(H_2O)_4^+$
EG	11.31	-	-	-	-
$EG(H_2O)$	11.39	10.33	-	-	-
$EG(H_2O)_2$	11.41	10.52	9.88	-	-
$EG(H_2O)_3$	11.29	10.43	9.96	9.54	-
$EG(H_2O)_4$	11.24	10.32	9.88	9.62	9.31

Table 4 shows that the size of the reactant EG water cluster does not determine the energy of the fragment cluster; rather, this energy is determined based on the size of the fragment cluster. The

calculated appearance energies in Table 4 show the experimentally seen downward trend as the size of the cluster increases and the roughly 1 eV drop in AE with the addition of one water to fragment m/z 31.

1,2- and 1,3-Propylene Glycol Water Clusters

As a comparison with EG and to see how the addition and placement of a methyl group affects photoionization, the VUV photoionization of 1,2-propylene glycol and 1,3-propylene glycol was performed. Similarly, to the EG experiments, the concentration of 1,2-propylene glycol to water and 1,3-propylene glycol to water was adjusted by changing the temperature of the nozzle as well as the pressure of the backing Ar (resulting in the peaks at m/z 40, Ar^+, and m/z 20, Ar^{2+}) gas. Mass spectra taken at photon energies of 10.5 and 12.5 eV with different mole fractions of 1,2- and 1,3-propylene glycol are shown in the SI in figures S11 (12PG, 10.5 eV), S12 (12PG, 12.5 eV), S13 (13PG, 10.5 eV), and S14 (13PG, 12.5 eV). The mass spectrum taken at 12.5 eV with 52% 1,2-propylene glycol is shown in Figure 12. Monomer and dimer protonated propylene glycol water clusters are indicated as well as the protonated propylene glycol trimer.

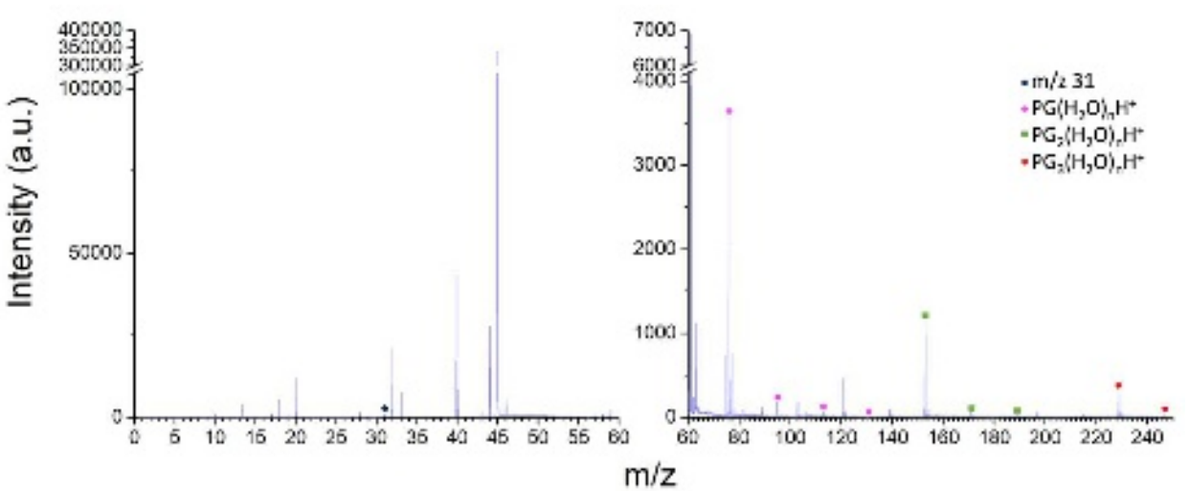

Figure 12 52% 1,2-propylene glycol mass spectrum taken at 12.5 eV showing monomer and dimer protonated propylene glycol water clusters as well as the protonated propylene glycol trimer. Propylene glycol has a mass of 76 amu.

The mass spectrum taken at 12.5 eV with 12% 1,3-propylene glycol is shown in Figure 13. The observed cluster series m/z 31$(H_2O)_n^+$, PG$(H_2O)_n^+$, and $PG_2(H_2O)_n^+$ are indicated.

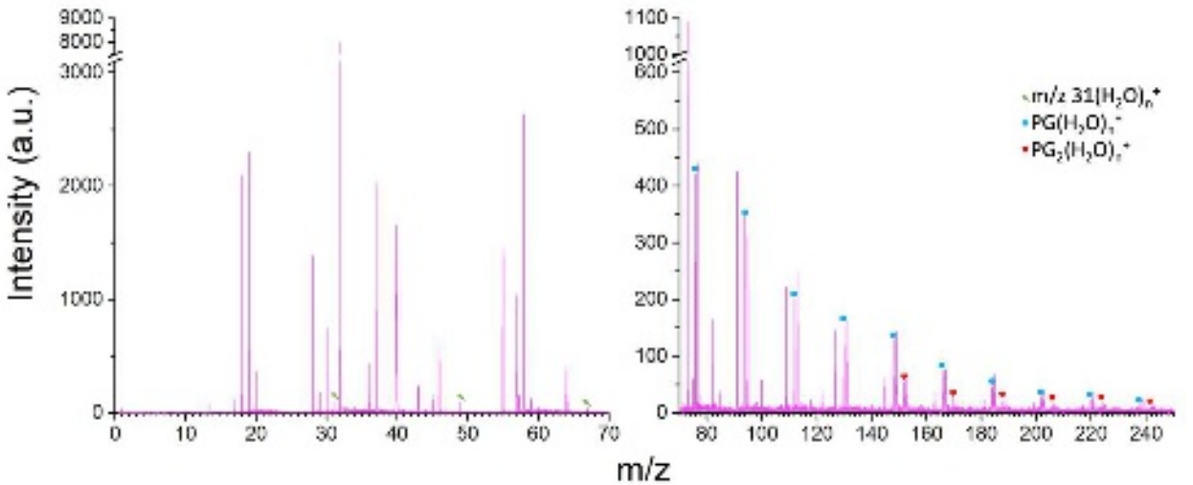

Figure 13 Mass spectrum taken with 12% 1,3-propylene glycol in the molecular beam at a photon energy of 12.5 eV. The cluster series for *m/z* 31$(H_2O)_n^+$, PG$(H_2O)_n^+$, and $PG_2(H_2O)_n^+$ are shown. Propylene glycol has a mass of 76 amu

The observed fragments from 1,2-propylene glycol are m/z 27, 29, 30, 31, 32, 33, 43, 44, 45, 61, and 63, which are the same as the fragments observed for EG, with the addition of m/z 63, which is attributed to protonated ethylene glycol. The observed fragments from 1,3-propylene glycol are m/z 27, 29, 30, 31, 32, 33, 43, 44, 45, 57, 59, 60, 75, which are similar to the other two diols, except for fragment m/z 61 and the addition of fragments m/z 57, 59, 60, and 75. These differences in fragmentation show that the addition of a methyl group as well as the location of this methyl group affect fragmentation. This methyl group affects hydrogen bonding in the cyclic transition state which then affects what fragments can form.

Figure 14 shows the sum of the cluster series as a function of the 1,2-propylene glycol mole fraction taken at 12.5 eV.

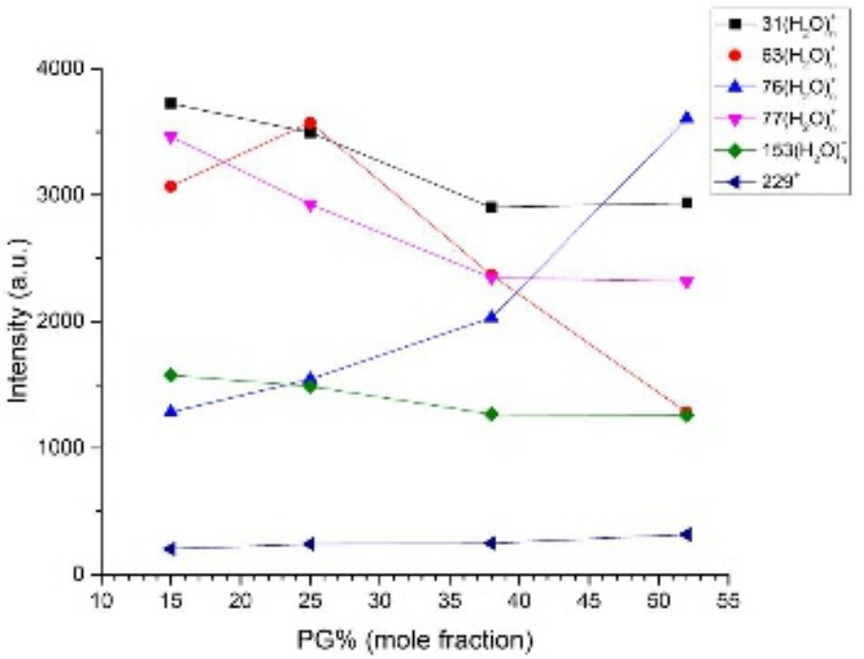

Figure 14 Sum of intensities of each cluster series as a function of 1,2-propylene glycol mole fraction, recorded at 12.5 eV.

Unlike what was seen with EG, as the concentration of 1,2-propylene glycol increases, the intensity for only 1,2-propylene glycol clusters and PG_3H^+ (m/z 229) increases while for all other clusters, the intensity decreases. This decreasing trend follows the depletion of water, which was also observed when glycerol water clusters were photoionized.[25] This decrease suggests that clusters m/z 31$(H_2O)_n^+$, m/z 63$(H_2O)_n^+$, m/z 77$(H_2O)_n^+$, and m/z 153$(H_2O)_n^+$ are directly involved in the photoionization dynamics of 1,2-propylene glycol water clusters.

Both propylene glycols are observed to form fragments of mass 31, just as was observed with EG. The photoionization intensity curves for fragments from 1,2-propylene glycol are shown in Figure S15 and for 1,2-propylene glycol water clusters in Figure S16. The photoionization intensity curves for fragments from 1,3-propylene glycol are shown in Figure S17 and for 1,3-propylene glycol water clusters in Figure S18. 1,2-propylene glycol does show a slight drop in appearance energy (given in Table 5) as more water clusters around it, but nothing like what was seen in EG. 1,3-propylene glycol does not show any drop in appearance energy (given in Table 5) with the addition of water to fragment m/z 31. This difference is attributed to the addition of a methyl group, and in the case of 1,3-propylene glycol, the location of the methyl group between the hydroxyl groups affecting hydrogen bonding and the transition state that forms before or during the photoionization process.

The appearance energies for forming clusters m/z 63$(H_2O)_n^+$, m/z 77$(H_2O)_n^+$, and m/z 153$(H_2O)_n^+$, given in Table 5, from 1,2-propylene glycol (seen in Figure S15 and S16) do not show the trend

observed with m/z 31 water clusters formed from ethylene glycol and 1,2-propylene glycol. This is due to differences in formation mechanisms. Fragment m/z31 forms when a C-C bond with hydroxyl groups attached to both carbons is broken. Fragment m/z 63 also forms through the breaking of a C-C bond, but in this case, only 1 carbon is attached to a hydroxyl group, the other is a methyl group. In the case of ethylene glycol, water can form hydrogen bonds with two hydroxyl groups, but can only form a hydrogen bond with one hydroxyl group when breaking off the methyl group to form m/z 63. The lack of change in appearance energy as the m/z 63$(H_2O)_n^+$ cluster increases in size may be due to this lessened hydrogen bonding which may affect the stabilization of the reaction. While the exact mechanism for the formation of fragment m/z 63 was not determined in this work, the lack of change in appearance energy as the cluster size increases lends support to the hypothesis that water stabilizes the formation of fragment m/z 31. The other cluster series, m/z 77$(H_2O)_n^+$ and m/z 153$(H_2O)_n^+$, do not form through fragmentation. m/z 77 is a protonated propylene glycol molecule and m/z 153 is a protonated propylene glycol dimer.

Table 5 Experimental appearance energies in eV of 1,2- and 1,3-propylene glycol clusters as well as observed fragments and fragment clusters taken at a propylene glycol mole fraction of 12% for 1,2- and 30% for 1,3-propylene glycol. The error is ±0.1. Using an effusive heater, the AE for 1,2-propylene glycol was found to be 9.80 ± 0.1 eV and that of 1,3-propylene glycol 9.75 ± 0.05 eV, which, within experimental error matches this data. This data is given in Table S1 in the SI. A - indicates that the signal-to-noise ratio was not sufficient to obtain a conclusive AE value. * indicates that the photoionization intensity curve has a low signal to noise resulting in high uncertainty in the AE value. The identity of the m/z # is indicated by square brackets.

12% 1,2-PG	AE (eV)	30% 1,3-PG	AE (eV)
m/z 27^+	9.6		
m/z 29^+	9.5		
m/z 30^+	10.5		
m/z 31^+	11.1	m/z 31^+	11.3
m/z 31$(H_2O)^+$	10.8	m/z 31$(H_2O)^+$	11.2
m/z 31$(H_2O)_2^+$	10.5	m/z 31$(H_2O)_2^+$	11.2*
m/z 31$(H_2O)_3^+$	10.4	m/z 31$(H_2O)_3^+$	-
m/z 31$(H_2O)_4^+$	10.1		
m/z 31$(H_2O)_5^+$	9.6		
m/z 31$(H_2O)_6^+$	9.5		
m/z 31$(H_2O)_7^+$	9.5		
m/z 31$(H_2O)_8^+$	9.5		
m/z 31$(H_2O)_9^+$	9.5*		
m/z 31$(H_2O)_{10}^+$	9.5*		
m/z 33^+	10.1		

m/z 43^+	10.0	m/z 43^+	10.2
m/z 44^+	10.1	m/z 44^+	10.2
m/z 45^+	10.3	m/z 45^+	10.0
m/z 63^+, [EGH]	9.6	m/z 57^+	10.7
m/z $63(H_2O)^+$	9.7	m/z 59^+	10.0
m/z $63(H_2O)_2^+$	9.5	m/z 60^+	10.0
m/z $63(H_2O)_3^+$	9.5	m/z 75^+	10.9
m/z $63(H_2O)_4^+$	9.5		
m/z 76^+, [PG]	9.7	m/z 76^+, [PG]	9.7
m/z $76(H_2O)^+$	9.5	m/z $76(H_2O)^+$	9.8
m/z $76(H_2O)_2^+$	9.5	m/z $76(H_2O)_2^+$	-
m/z 77^+, [PGH]	9.8	m/z 77^+, [PGH]	9.8
m/z $77(H_2O)^+$	10.1	m/z $77(H_2O)^+$	9.8
m/z $77(H_2O)_2^+$	10.0	m/z $77(H_2O)_2^+$	9.8*
m/z $77(H_2O)_3^+$	10.0	m/z $77(H_2O)_3^+$	-
m/z $77(H_2O)_4^+$	9.9	m/z 152^+, [PG_2]	9.7
m/z $77(H_2O)_5^+$	10.0	m/z $152(H_2O)^+$	9.6*
m/z $77(H_2O)_6^+$	10.0	m/z $152(H_2O)_2^+$	-
m/z 153^+, [PG_2H]	9.4	m/z 153^+, [PG_2H]	9.6
m/z $153(H_2O)^+$	9.4	m/z $153(H_2O)^+$	9.6*
m/z $153(H_2O)_2^+$	9.4		
m/z $153(H_2O)_3^+$	9.5		
m/z $153(H_2O)_4^+$	9.5*		
m/z $153(H_2O)_5^+$	9.5*		
m/z 229^+, [PG_3H]	9.5*	m/z 229^+, [PG_3H]	9.7

For 1,3-propylene glycol, a similar trend in decreasing AE was observed for certain fragment water clusters formed when glycerol water clusters were photoionized. Fragments m/z 61, 62, and 74 were found to form clusters with water. No trend was observed for fragment m/z 31, as this fragment was not detected, though the formation of this fragment was predicted, by theory, to be barrierless.[25] The appearance energies of the fragment clusters m/z $62(H_2O)_n^+$ and m/z $74(H_2O)_n^+$ are close to that of pure glycerol (AE = 9.4 eV) and show a change of 0.1 eV, which is within the experimental error, as more water molecules cluster around the fragment. Fragment m/z 61 from glycerol showed a decrease in appearance energy of 0.3 eV with the addition of 1 water molecule, which is larger than was seen with the other fragments but small compared with what was seen with fragment m/z 31 from EG. The decrease in energy with the addition of water

was on the order of that observed for the fragmentation of 1,2-propylene glycol. For comparison, the optimized geometries of neutral (top) and cation (bottom) EG, 1,2-propylene glycol (12PG), 1,3-propylene glycol (13PG), and glycerol (GLY)[25] are shown in Figure 15. These were optimized with Q-Chem at the ωB97X-V/def2-TZVPPD level of theory.

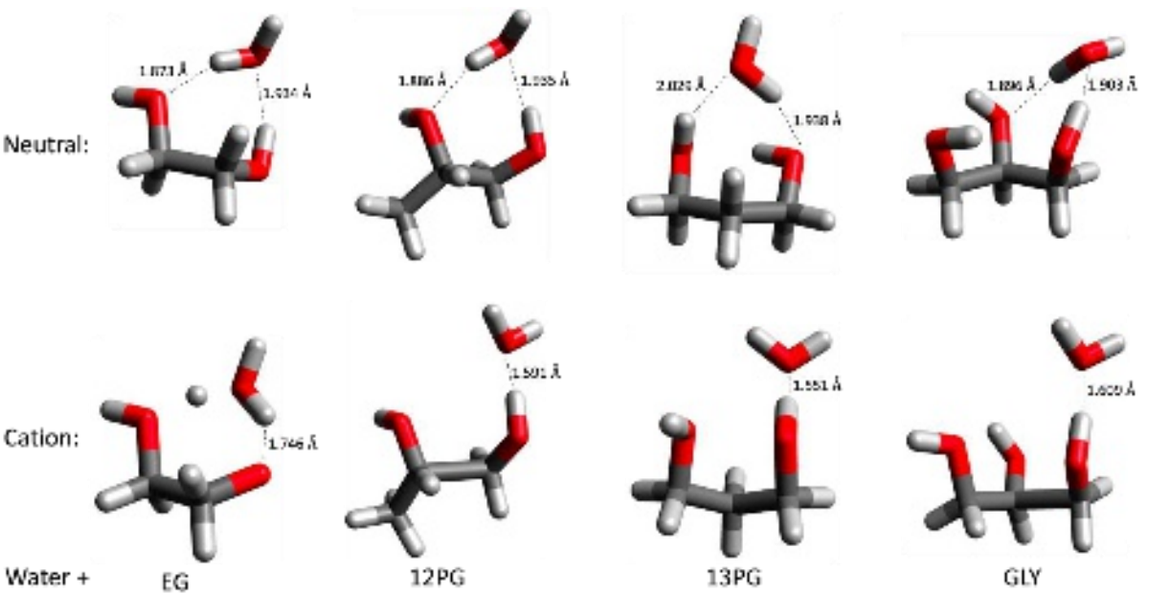

Figure 15 Optimized geometry of neutral (top row) and cation (bottom row) ethylene glycol (EG), 1,2-propylene glycol (12PG), 1,3-propylene glycol (13PG), and glycerol (GLY)[25] with the hydrogen bond lengths given. The optimization was done using Q-Chem at the ωB97X-V/def2-TZVPPD level of theory.

Figure 15 shows how the hydrogen bonding between water and alcohol changes with ionization. Before ionization, all alcohols form at least two hydrogen bonds with water. These hydrogen bonds are between 1.87 and 2.1 Å. Upon ionization, one hydrogen bond between all alcohols and water is severed. When ionized, the alcohols 1,2-propylene glycol, 1,3-propylene glycol, and glycerol act as hydrogen bond donors, and the water drifts closer to one hydroxyl group. For 1,2-propylene glycol, the hydrogen bond that remains goes from 1.935 Å to 1.591 Å, and the severed hydrogen bond is 1.886 Å long. For 1,3-propylene glycol, the hydrogen bond that remains goes from 1.938 Å to 1.551 Å, and the severed hydrogen bond is 2.029 Å long. For glycerol, the hydrogen bond that remains goes from 1.903 Å to 1.609 Å, and the severed hydrogen bond is 1.896 Å long. Ethylene glycol, which contains one fewer methyl group than the propylene glycols and one fewer methyl group and hydroxyl group than glycerol, undergoes a proton transfer when ionized and therefore acts as a hydrogen bond acceptor rather than donor as the other alcohols did. This proton is shared between the hydroxyl group and water, similar to a Zundel ion. Ionized ethylene glycol exhibits a slightly higher propensity to bind to water than the other larger alcohols given the hydrogen bond network connecting the oxygens of ethylene glycol via water and the lone proton.

The fragmentation process, upon VUV photoionization, of pure glycerol occurs through either a six-membered hydrogen transfer transition state forming a stable ternary intermediate or through

elongation of the C-C bond. Cyclic hydrogen bond transition structures were found to be involved in the fragmentation process, upon VUV photoionization, of glycerol water clusters[25] and deoxyribose.[24] The fragmentation of the diol water clusters is proposed to occur through a similar cyclic hydrogen bond transition state as well as via C-C bond elongation. The cyclic hydrogen bond transition state that can form is dependent upon the location of the hydroxyl groups on the diol, which explains the difference in fragments observed for the three diols as well as the difference in appearance energy trends between these diols.

The combination of diol with water is found to change the ionization mechanism for both the water and the diol. In general, cationic diols are found to have a lower propensity for binding to water than neutral diols, as shown in Figure 15, by the severing of one hydrogen bond when ionized. The remaining hydrogen bond is shorter and stronger than either hydrogen bond before ionization, which is attributed to a stronger binding energy between water and a cation than between water and a neutral molecule, as was found in the binding energy study of neutrals, radicals, and ions.[39] By understanding the effect water has upon ionization mechanisms and fragmentation of the diols EG, 1,2-propylene glycol, and 1,3-propylene glycol, reactions occurring on the icy mantles of dust grains in the ISM can be better understood and predicted. Based upon these findings, cationic diols and alcohols in general will form fewer hydrogen bonds with water when ionized, but a stronger water-ion interaction will favor fragmentation through breaking the C-C bond when cationic diols are surrounded by water. This is supported by the lowering of appearance energy as the number of waters clustering around fragment m/z 31 increases. These findings are based on small clusters of water surrounding the alcohol. To fully understand the reaction dynamics occurring in the ISM, further studies involving ice and these diols along with calculations simulating a full surface of water are needed, such as has been done with some polycyclic aromatic hydrocarbons trapped onto cryogenic water-ice.[41]

Conclusions

A better understanding of the hydrogen bonding formed between diol alcohols and water can further their use as cryoprotectants in biological systems[4], superconductors, sensors [5,6], and batteries[7,8] as well as shed light into reactions potentially occurring on the icy mantles of dust grains. As a proxy for these systems, EG, 1,2-propylene glycol, and 1,3-propylene glycol water clusters were photoionized using tunable VUV radiation (in the range of 9.0 to 12.5 eV), and the products were detected using reflectron time-of-flight mass spectrometry. Water clustered around the diols as well as fragments of the diols were detected, indicating that through the fragmentation process, not all water surrounding the diol evaporates. The detected fragments differed for the three diols. EG and 1,2-propylene glycol exhibited similar fragmentation both forming fragments m/z 31, 32, 33, 43, 44, 45, 61, and 1,2-propylene glycol formed fragment m/z 63. 1,3-propylene glycol exhibited somewhat different fragmentation forming fragments m/z 31, 32, 43, 44, 45, 57, 59, 60, 75. This difference is due to the addition and location of the methyl group. From the mass spectra, photoionization intensity curves were determined, and from this, the appearance energies (AE) for the clusters were obtained. AE for the unfragmented diol water

clusters was found to show little variation with cluster size. A small decrease in AE was observed as cluster size increased, similar to what was observed with glycerol water clusters.[25] The formation of fragment clusters through dissociative ionization was found to be affected by the number of methyl groups and the placement of hydroxyl groups with respect to these methyl groups. In the case of EG, forming m/z 31$(H_2O)_n^+$ takes roughly 1 eV less energy than forming m/z 31. With the addition of 1 methyl group to the end of EG, forming 1,2-propylene glycol, fragmentation to produce m/z 31$(H_2O)_n^+$ takes 0.3 eV less than producing m/z 31. When the hydroxyl group is moved to the added methyl, in the case of 1,3-propylene glycol, no change in energy needed to form m/z 31$(H_2O)_n^+$ versus m/z 31 is observed. This indicates that methyl group and hydroxyl group location play a large role in the energy needed to undergo dissociative photoionization when water is present. This is attributed to the formation of a cyclic hydrogen-bonded transition state, similar to that observed for glycerol water clusters and deoxyribose.

The formation of complex organic molecules of astronomical relevance, such as aromatic hydrocarbons, alcohols, ethers, aldehydes, enols, ketones, and carboxylic acids, has been observed experimentally through ionizing radiation of interstellar analog ices.[42-43] Through this work, mechanisms for the formation of COMs in star-forming regions can be proposed. The temperature-programmed desorption of n- and i-propanol from an ice surface was determined using broad-band millimeter-wave rotational spectroscopy, indicating that desorption is highly conformer-specific.[44] Low-temperature oxidation of the ice-embedded alcohol's methanol, ethanol, 1-propanol, 2-propanol, 1-butanol, and t-butanol via a 1 MeV proton beam at ~20 K was performed, and the products were identified via infrared spectroscopy. The peak positions of the products, which are aldehydes and ketones, could be used when searching the ISM with IR-capable instruments such as the James Webb Space Telescope.[45] A further infrared spectroscopy study looked at X-ray and vacuum ultraviolet radiation-induced transformation of ethanol, both deuterated and undeuterated, in solid inert matrices of Ne, Ar, Kr, and Xe at 4.4 K. The radiation produced dehydrogenation products, with variation in the observed products based upon the radiation source, whether X-ray or VUV.[46] By combining information from these and other ice chemistry studies with the knowledge of hydrogen bond networks formed between alcohols and water discussed in this paper, greater insight into the processes and reactions occurring on space ice in the ISM can be achieved.

The picture of these hydrogen bond networks also provides insights into how to form better chemical systems, such as superconductors and batteries, and for use in biological systems. The hydrogen bonds formed between alcohols, most often ethylene glycol, and water cause a glassy state resulting in anti-freezing properties. These properties are being applied to biological systems, such as in the case of the stabilization of proteins[4], as well as in superconductors[5-6] and batteries[7,8] to produce useful devices at low temperatures. Concentration and temperature effects on aqueous ethylene glycol solutions were studied using Raman correlation spectroscopy. With increasing concentration of ethylene glycol came weakening of the hydrogen bonds formed between water as well as a decrease in a solid ice Raman peak as the temperature was lowered[47]. A further Raman study looking at aqueous EG and 13PG solutions found that the concentration of the diol only weakly influenced the band spectra, with a small increase in gauche confirmation relative to the O-C-C-O torsional angle as concentration increased. The finding of this slight gauche preference when in the presence of water was supported by DFT-simulated Raman spectra.[48]

Molecular dynamics simulations using an empirical force field further support the finding of a preferred gauche confirmation for EG when in an aqueous solution. This preference is attributed to a slightly higher number of hydrogen bonds that can form in this conformation.[49]

While some experimentation and theory work has been done to better understand and visualize aqueous diol solutions, there are still many gaps. The hydrogen bonding networks reported in this work, in figures 5 through 7 and 15, begin to fill some of these gaps and help pave the way for further experiments to fully understand these interactions and apply the obtained knowledge to create better chemical and biological systems.

Supplementary Material

Photoionization intensity curves of fragments and clusters of ethylene glycol, 1,2 and 1,3 propylene glycol water clusters. Intensities of fragment masses and clusters as a function of cluster size and photon energy (eV). Mass spectra of 1,2 and 1,3 propylene glycol water clusters and fragments at various propylene glycol mole fractions. Appearance energies of 1,2 and 1,3 propylene glycol and fragments recorded in an effusive source. Cartesian coordinates of structures calculated in this work.

Acknowledgments

We would like to acknowledge Qiao N. Ruan for the use of his propylene glycol appearance energy data as well as thank Sander Lemmens for helpful discussion regarding this work. This work is supported by the Gas Phase Chemical Physics Program, in the Chemical Sciences Geosciences and Biosciences Division of the Office of Basic Energy Sciences of the U.S. Department of Energy under Contract No. DE-AC02-05CH11231 and the U.S. Department of Energy, Office of Science, Office of Workforce Development for Teachers and Scientists, Office of Science Graduate Student Research (SCGSR) program (Contract No. DE-SC0014664). This research used resources from the Advanced Light Source, which is a DOE Office of Science User Facility under Contract No. DE-AC02-05CH11231.

Contributions:

Anna Wannenmacher: Writing/Original Draft Preparation, Writing/Review Editing, Formal Analysis, Visualization, Conceptualization (equal)

Wenchao Lu: Data Curation

Chandika Amarasinghe: Data Curation

Frank Cerasoli: Resources (supporting)

Davide Donadio: Resources(supporting), review/editing, analysis (supporting), theory supervision

Musahid Ahmed: Conceptualization (equal), Supervision (lead), Writing/Review Editing, Funding Acquisition (lead)

References:

1. Brouillet, N.; Despois, D.; Lu, X.-H.; Baudry, A.; Cernicharo, J.; Bockelée-Morvan, D.; Crovisier, J.; Biver, N., Antifreeze in the Hot Core of Orion. *A&A* 2015, *576*, A129.
2. Rivilla, V. M.; Beltrán, M. T.; Cesaroni, R.; Fontani, F.; Codella, C.; Zhang, Q., Formation of Ethylene Glycol and Other Complex Organic Molecules in Star-Forming Regions⋆. *A&A* 2017, *598*, A59.
3. Moore, M. H.; Hudson, R. L., Production of Complex Molecules in Astrophysical Ices. *Proc. Int. Astron. Union.* 2005, *1*, 247-260.
4. Tejaswi Naidu, K.; Prakash Prabhu, N., An Able-Cryoprotectant and a Moderate Denaturant: Distinctive Character of Ethylene Glycol on Protein Stability. *J. Biomol. Struct. Dyn.* 2022, *40*, 820-832.
5. Yang, L.; Chen, M.; Wu, T. Z.; Niu, L.; Zeng, L.; Feng, G., Low-Temperature Electrolytes for Electrochemical Energy Storage Devices: Bulk and Interfacial Properties. *KFPE* 2023, *8* 033005.
6. Tian, G. K.; Chai, P. Z.; Yu, H.; Zheng, W. X., A Low-Cost Dilute Aqueous Hybrid Electrolyte for Low-Temperature Supercapacitors. *J. Solid State Electrochem.* 2023, *27*, 2771-2777.
7. Zhang, H. B.; Yu, Y.; Zuo, Y. X.; Zuo, C. C.; Lu, D. H.; Zhao, Z. F., Freeze-Resistant and Robust Gel Electrolyte for Flexible Aluminum-Air Batteries. *Ion* 2023, *29*, 3087-3096.
8. Zheng, Z. Y.; Shi, W. H.; Zhou, X. L.; Zhang, X. P.; Guo, W. L.; Shi, X. Y.; Xiong, Y.; Zhu, Y. S., Agar-Based Hydrogel Polymer Electrolyte for High-Performance Zinc-Ion Batteries at All Climatic Temperatures. *ISCIENCE* 2023, *26*, 106437.
9. R. J, S.; Rakhee, C.; S. C, M., Dielectric Behaviour of Propylene Glycol-Water Mixtures Studied by Time Domain Reflectometry. *Mol. Phys.* 2001, *99*, 1805-1812.
10. Malcolm, G. N.; Rowlinson, J. S., The Thermodynamic Properties of Aqueous Solutions of Polyethylene Glycol, Polypropylene Glycol and Dioxane. *Trans. Faraday Soc.* 1957, *53*, 921--931.
11. Sengwa, R. J., A Comparative Dielectric Study of Ethylene Glycol and Propylene Glycol at Different Temperatures. *J. Mol. Liq.* 2003, *108*, 47--60.
12. Villamanan, M. A.; Gonzalez, C.; Van Ness, H. C., Excess Thermodynamic Properties for Water/Ethylene Glycol. *JCED* 1984, *29*, 427--429.
13. Chaudhari, A.; Lee, S.-L., A Computational Study of Microsolvation Effect on Ethylene Glycol by Density Functional Method. *Chem. Phys.* 2004, *120*, 7464-7469.
14. Gubskaya, A. V.; Kusalik, P. G., Molecular Dynamics Simulation Study of Ethylene Glycol, Ethylenediamine, and 2-Aminoethanol. 2. Structure in Aqueous Solutions. *J. Phys. Chem. A* 2004, *108*, 7165--7178.
15. Gubskaya, A. V.; Kusalik, P. G., Molecular Dynamics Simulation Study of Ethylene Glycol, Ethylenediamine, and 2-Aminoethanol. 1. The Local Structure in Pure Liquids. *J. Phys. Chem. A* 2004, *108*, 7151--7164.

16. Naganathappa, M.; Chaudhari, A., Mono, Di, Tri, and Tetraethylene Glycol: Spectroscopic Characterization Using Density Functional Method and Experiment. *Vib. Spectrosc.* **2018**, *95*, 7-15.
17. Ying, W.; Fabing, L.; Wenhui, F.; Chenglin, S.; Zhiwei, M., Study of Hydrogen Bonding Interactions in Ethylene Glycol-Water Binary Solutions by Raman Spectroscopy. *Spectrochim. Acta - A: Mol. Biomol.* **2021**, *260*, 119916.
18. Chen, Y.; Ozaki, Y.; Czarnecki, M. A., Molecular Structure and Hydrogen Bonding in Pure Liquid Ethylene Glycol and Ethylene Glycol–Water Mixtures Studied Using Nir Spectroscopy. *PCCP* **2013**, *15*, 18694-18701.
19. Ng, C.-Y., Vacuum Ultraviolet Spectroscopy and Chemistry by Photoionization and Photoelectron Methods. *Annu. Rev. Phys. Chem.* **2002**, *53*, 101-140.
20. Kostko, O.; Bandyopadhyay, B.; Ahmed, M., Vacuum Ultraviolet Photoionization of Complex Chemical Systems. *Annu. Rev. Phys. Chem* **2016**, *67*, 19-40.
21. Belau, L.; Wilson, K. R.; Leone, S. R.; Ahmed, M., Vacuum Ultraviolet (Vuv) Photoionization of Small Water Clusters. *J. Phys. Chem. A* **2007**, *111*, 10075-10083.
22. Kostko, O.; Belau, L.; Wilson, K. R.; Ahmed, M., Vacuum-Ultraviolet (Vuv) Photoionization of Small Methanol and Methanol–Water Clusters. *J. Phys. Chem. A* **2008**, *112*, 9555-9562.
23. Bell, F.; Ruan, Q. N.; Golan, A.; Horn, P. R.; Ahmed, M.; Leone, S. R.; Head-Gordon, M., Dissociative Photoionization of Glycerol and Its Dimer Occurs Predominantly Via a Ternary Hydrogen-Bridged Ion–Molecule Complex. *J. Am. Chem. Soc.* **2013**, *135*, 14229-14239.
24. Ghosh, D.; Golan, A.; Takahashi, L. K.; Krylov, A. I.; Ahmed, M., A Vuv Photoionization and Ab Initio Determination of the Ionization Energy of a Gas-Phase Sugar (Deoxyribose). *J. Phys. Chem. Lett.* **2012**, *3*, 97-101.
25. Lu, W.; Mackie, C. J.; Xu, B.; Head-Gordon, M.; Ahmed, M., A Computational and Experimental View of Hydrogen Bonding in Glycerol Water Clusters. *J. Phys. Chem. A* **2022**, *126*, 1701-1710.
26. Wang, H.; Guan, J.; Gao, J.; Li, Y.; Zhang, J.; Shan, X.; Wang, Z., Discriminating between the Dissociative Photoionization and Thermal Decomposition Products of Ethylene Glycol by Synchrotron Vuv Photoionization Mass Spectrometry and Theoretical Calculations. *PCCP* **2022**, *24*, 26915-26925.
27. Kumar, R. M.; Baskar, P.; Balamurugan, K.; Das, S.; Subramanian, V., On the Perturbation of the H-Bonding Interaction in Ethylene Glycol Clusters Upon Hydration. *J. Phys. Chem. A* **2012**, *116*, 4239-4247.
28. Belau, L.; Wilson, K. R.; Leone, S. R.; Ahmed, M., Vacuum-Ultraviolet Photoionization Studies of the Microhydration of DNA Bases (Guanine, Cytosine, Adenine, and Thymine). *J. Phys. Chem. A* **2007**, *111*, 7562-7568.
29. Ahmed, M.; Kostko, O., From Atoms to Aerosols: Probing Clusters and Nanoparticles with Synchrotron Based Mass Spectrometry and X-Ray Spectroscopy. *PCCP* **2020**, *22*, 2713-2737.
30. Pracht, P.; Bohle, F.; Grimme, S., Automated Exploration of the Low-Energy Chemical Space with Fast Quantum Chemical Methods. *PCCP* **2020**, *22*, 7169-7192.
31. Evgeny, E., et al., Software for the Frontiers of Quantum Chemistry: An Overview of Developments in the Q-Chem 5 Package. *J. Chem. Phys.* **2021**, *155*, 084801.
32. Narbe, M.; Martin, H.-G., Thirty Years of Density Functional Theory in Computational Chemistry: An Overview and Extensive Assessment of 200 Density Functionals. *Mol. Phys.* **2017**, *115*, 2315-2372,.

33. Nicolas, C.; Shu, J.; Peterka, D. S.; Hochlaf, M.; Poisson, L.; Leone, S. R.; Ahmed, M., Vacuum Ultraviolet Photoionization of C3. *J. Am. Chem. Soc.* 2006, *128*, 220-226.
34. Szabo, A.; Ostlund, N. S., *Modern Quantum Chemistry: Introduction to Advanced Electronic Structure Theory, 1st Ed.*, 1st ed. ed.; Dover Publications, 1996.
35. Xu, B.; Stein, T.; Ablikim, U.; Jiang, L.; Hendrix, J.; Head-Gordon, M.; Ahmed, M., Probing Solvation and Reactivity in Ionized Polycyclic Aromatic Hydrocarbon–Water Clusters with Photoionization Mass Spectrometry and Electronic Structure Calculations. *Faraday Discuss.* 2019, *217*, 414-433.
36. Amir, G.; Musahid, A., Molecular Beam Mass Spectrometry with Tunable Vacuum Ultraviolet (Vuv) Synchrotron Radiation. *JoVE* 2012, *68*, e50164.
37. Khistyaev, K.; Golan, A.; Bravaya, K. B.; Orms, N.; Krylov, A. I.; Ahmed, M., Proton Transfer in Nucleobases Is Mediated by Water. *J. Phys. Chem. A* 2013, *117*, 6789-6797.
38. Jagannath, P.; Arnab, P.; Ranga, S., Thermodynamic Properties of Forming Methanol-Water and Ethanol-Water Clusters at Various Temperatures and Pressures and Implications for Atmospheric Chemistry: A Dft Study. *Chemosphere* 2021, *272*, 129846.
39. Hendrix, J.; Bera, P. P.; Lee, T. J.; Head-Gordon, M., Quantum Chemical Exploration of the Binding Motifs and Binding Energies of Neutral Molecules, Radicals and Ions with Small Water Clusters: Characterisation and Astrochemical Implications. *Mol. Phys.*, e2252100.
40. Lu, W.; Metz, R. B.; Troy, T. P.; Kostko, O.; Ahmed, M., Exciton Energy Transfer Reveals Spectral Signatures of Excited States in Clusters. *PCCP* 2020, *22*, 14284-14292.
41. Antti, L.; Laura, I. T.-O.; Murthy, S. G., Visible-Light Photoionization of Aromatic Molecules in Water-Ice: Organic Chemistry across the Universe with Less Energy. *Chem. Phys. Lett.* 2021, *778*, 138814.
42. Turner, A. M.; Kaiser, R. I., Exploiting Photoionization Reflectron Time-of-Flight Mass Spectrometry to Explore Molecular Mass Growth Processes to Complex Organic Molecules in Interstellar and Solar System Ice Analogs. *Acc. Chem. Res.* 2020, *53*, 2791-2805.
43. Zhu, C.; Frigge, R.; Bergantini, A.; Fortenberry, R. C.; Kaiser, R. I., Untangling the Formation of Methoxymethanol (Ch3och2oh) and Dimethyl Peroxide (Ch3ooch3) in Star-Forming Regions. *ApJ* 2019, *881*, 156.
44. Borengasser, Q.; Hager, T.; Kanaherarachchi, A.; Troya, D.; Broderick, B. M., Conformer-Specific Desorption in Propanol Ices Probed by Chirped-Pulse Millimeter-Wave Rotational Spectroscopy. *J. Phys. Chem. Lett.* 2023, *14*, 6550-6555.
45. Hudson, R. L.; Moore, M. H., Interstellar Ices and Radiation-Induced Oxidations of Alcohols. *ApJ* 2018, *857*, 89.
46. Zasimov, P. V.; Sanochkina, E. V.; Tyurin, D. A.; Feldman, V. I., Radiation-Induced Transformations of Matrix-Isolated Ethanol Molecules at Cryogenic Temperatures: An Ftir Study. *PCCP* 2023, *25*, 21883-21896.
47. Yang, B.; Ren, P.; Xing, L.; Sun, C.; Men, Z., Hydrogen-Bond Dynamics and Water Structure in Aqueous Ethylene Glycol Solution Via Two-Dimensional Raman Correlation Spectroscopy. *J. Phys. Chem. Lett.* 2023, *14*, 1641-1649.
48. Liubimovskii, S. O., et al., Raman Structural Study of Ethylene Glycol and 1,3-Propylene Glycol Aqueous Solutions. *Spectrochim Acta A Mol Biomol Spectrosc* 2023, *285*, 121927.

49. Gaur, A.; Balasubramanian, S., Conformer Selection Upon Dilution with Water: The Fascinating Case of Liquid Ethylene Glycol Studied Via Molecular Dynamics Simulations**. *ChemistryOpen* **2023**, *12*, e202200132.